Title
Oxygenated Mesoproterozoic lake revealed through magnetic mineralogy

Journal
Proceedings of the National Academy of Sciences of the United States of America, 115(51)

ISSN
0027-8424

Authors
Slotznick, Sarah P
Swanson-Hysell, Nicholas L
Sperling, Erik A

Publication Date
2018-12-18

DOI
10.1073/pnas.1813493115

An oxygenated Mesoproterozoic lake revealed through magnetic mineralogy

Sarah P. Slotznick[a], **Nicholas L. Swanson-Hysell**[a], **and Erik A. Sperling**[b]

[a]Department of Earth and Planetary Science, University of California, Berkeley, CA 94720 USA; [b]Department of Geological Sciences, Stanford University, Stanford, CA 94305 USA

This manuscript is the author's final version of Slotznick et al. (2018) published in PNAS https://doi.org/10.1073/pnas.1813493115.

Terrestrial environments have been suggested as an oxic haven for eukaryotic life and diversification during portions of the Proterozoic Eon when the ocean was dominantly anoxic. However, iron speciation and Fe/Al data from the ca. 1.1 billion year old Nonesuch Formation, deposited in a large lake and bearing a diverse assemblage of early eukaryotes, are interpreted to indicate persistently anoxic conditions. To shed light on these distinct hypotheses, we analyzed two drill-cores spanning the transgression into the lake and its subsequent shallowing. While the proportion of highly reactive to total iron (Fe_{HR}/Fe_T) is consistent through the sediments and typically in the range taken to be equivocal between anoxic and oxic conditions, magnetic experiments and petrographic data reveal that iron exists in three distinct mineral assemblages resulting from an oxycline. In the deepest waters, reductive dissolution of iron oxides records an anoxic environment. However, the remainder of the sedimentary succession has iron oxide assemblages indicative of an oxygenated environment. At intermediate water depths, a mixed-phase facies with hematite and magnetite indicates low oxygen conditions. In the shallowest waters of the lake, nearly every iron oxide has been oxidized to its most oxidized form, hematite. Combining magnetics and textural analyses results in a more nuanced understanding of ambiguous geochemical signals and indicates that for much of its temporal duration, and throughout much of its water column, there was oxygen in the waters of Paleolake Nonesuch.

Proterozoic | oxygen | iron speciation | lacustrine environments | eukaryotic evolution

Following the origin of eukaryotic life in the Paleoproterozoic Era (2500-1600 Ma), eukaryotic diversity is interpreted to have remained relatively low in marine environments throughout the Mesoproterozoic Era (1600-1000 Ma) until ca. 800 Ma during the Neoproterozoic Era (1, 2). A hypothesis to explain delayed eukaryotic diversification is that marine environments in a relatively low oxygen world were prone to the upwelling of anoxic, and sometimes sulfidic, waters from widespread oxygen minimum zones (1, 3–5), but see (6). The inhibitory effect of low-oxygen waters on aerobic eukaryotic life holds true whether hypoxic conditions were caused by low atmospheric oxygen–as commonly assumed–or from shallow remineralization of sinking organic matter (7). This potential challenge for eukaryotic life in the marine realm has led to the suggestion that oxygenated terrestrial environments may have been cradles of eukaryotic diversification (4, 8).

Microfossils recovered from the Torridonian sequence of Scotland and the Nonesuch Formation of North America have been interpreted to indicate that by ca. 1.1 Ga freshwater habitats were colonized by eukaryotes as well as cyanobacteria (4, 8, 13). Recovered specimens from the Nonesuch Formation include *Valeria lophostriata* (4), which is considered to be diagnostically eukaryotic as the complex wall morphologies and microstructures could not be generated by an organism that does not have a cytoskeleton and endomembrane system (14). The microfossil record of the Nonesuch Formation has been further interpreted to indicate the presence of more than 50 different species (4). This record is argued to be more diverse than similar-aged marine assemblages which leads to the interpretation that lacustrine environments with stable oxygenated waters may have been more hospitable to eukaryotic evolution than marine ones (4). Early oxygenation of lacustrine environments during the Mesoproterozoic has also been proposed based on large sulfur isotope fractionations from sedimentary rocks of the Stoer and Torridon groups that were interpreted to have resulted from oxidative sulfur cycling (15). However, this interpretation is equivocal given that such fractionation can arise without oxidative cycling (16, 17).

The chemistry and mineralogy of iron and oxygen in the environment are tightly interwoven, and iron-based geochemical proxies are amongst the most mature available for gaining insight into local redox conditions (18). Iron speciation measurements, combined with total iron to aluminum ratios (Fe_T/Al), have been performed on the Nonesuch Formation in the Presque Isle Syncline and used to infer persistent water-column anoxia throughout Paleolake Nonesuch (11). This finding was extrapolated to terrestrial environments as a whole in the Mesoproterozoic, thereby challenging the interpretation of such environments as a potential locus of aerobic Proterozoic eukaryotic evolution (11). However, published bulk-rock iron speciation data are not entirely straightforward to interpret.

Significance Statement

Constraining oxygen levels and redox chemistry of Proterozoic oceans and lakes is vital for placing environmental constraints on early aerobic eukaryotic evolution. Most recent work has utilized iron-based geochemical proxies—however, interpretation of such measurements can be difficult due to uncertainties related to baselines for lake sediments and equivocal zones associated with empirically-calibrated proxies. We integrate magnetic, geochemical, and microscale imaging techniques to analyze the iron mineralogy of 1.1 billion-year-old Paleolake Nonesuch, one of the few lacustrine records of this era. With these methods, we resolve ambiguous geochemical signals and document an oxycline with oxygenated shallow waters and decreasing oxygen with depth. These results indicate a stable oxygenated environment in the terrestrial realm 1.1 billion years ago.

S.S. and N.S.-H. designed the research, studied and sampled the cores, conducted rock magnetic experiments and analyzed associated data, and drafted the figures; S.S. conducted microscale textural analysis; E.S. developed geochemical data; S.S., N.S.-H. and E.S wrote the paper.

The authors declare no conflict of interest.

[1]To whom correspondence should be addressed. E-mail: sslotzberkeley.edu.

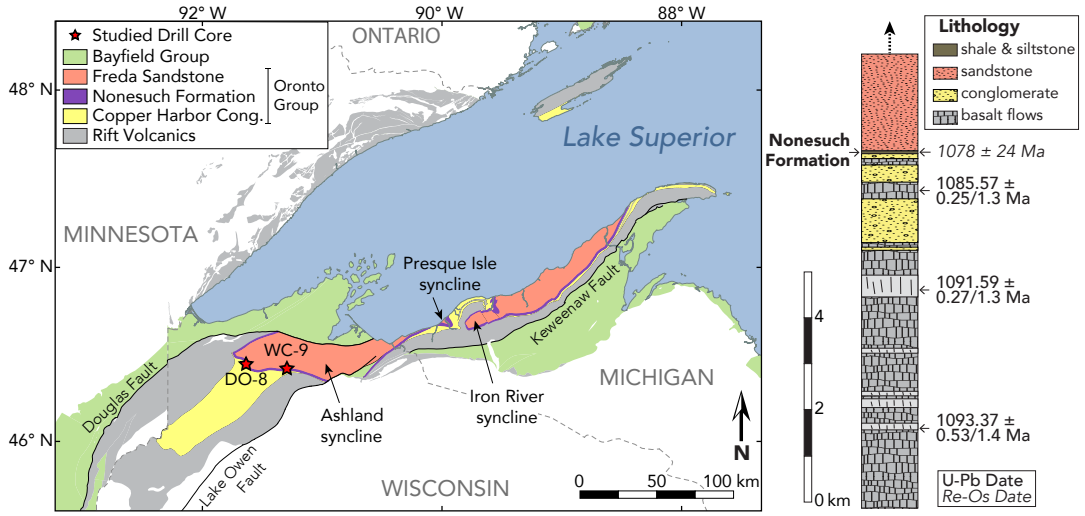

Fig. 1. Geologic map and summary stratigraphy of the Nonesuch Formation and other units from within the Midcontinent Rift. The geological data on the map are from (9) and the stratigraphic column from (10). The Re-Os date for the Nonesuch Shale is shown in italics with 2σ uncertainty (11). The U-Pb dates (10, 12) are shown with 2σ uncertainties (X/Y) that include analytical uncertainty alone (X) and include tracer and decay constant uncertainty (Y) for comparison with the Re-Os date. Cores studied in this work from the Ashland Syncline (DO-8 and WC-9) are shown with red stars.

The strength of the iron speciation proxy lies in its empirical calibration in modern marine sediments, allowing for the identification of authigenic reactive iron enrichments (resulting from anoxic water column processes) above an oxic baseline (the reactive iron delivered through detrital processes). There are few baseline data from lacustrine settings, and the delivery of iron to different lakes can be highly variable (19). Further, most of the existing iron speciation values from the Nonesuch Formation fall not in the clearly defined oxic or anoxic fields but in the 'possibly anoxic' area of iron speciation interpretive space (18). Given these ambiguities, new approaches to harness the redox information contained in the sedimentary iron record will have high utility in lacustrine rocks and other sediments where established proxies like iron speciation are ambiguous. This study pairs rock magnetics, geochemistry, and microscopy to develop a more detailed picture of assemblages of iron oxides and sulfides in Paleolake Nonesuch. These data reveal distinct depth-dependent mineralogical facies associated with the oxycline of this 1.1 billion year old lake. These facies are also seen within iron speciation extractions, but are obscured if these geochemical data are interpreted solely on the basis of the traditional anoxia proxy of Fe_{HR}/Fe_T (highly reactive iron to total iron) in conjunction with Fe_T/Al.

Paleolake Nonesuch. Following a prolonged interval of voluminous volcanic activity within the North American Midcontinent Rift, sedimentation within a thermally subsiding basin led to the deposition of sedimentary rocks of the Oronto Group (20). The Oronto Group commences with the Copper Harbor Conglomerate, which represents a terrestrially-deposited alluvial fan and fluvial sediments (21). Locally, on the Keweenaw Peninsula, lava flows of the Lake Shore Traps erupted within the Copper Harbor Conglomerate and an andesitic lava within these flows has an U-Pb date of 1085.57 ± 0.25/1.3 Ma (Fig. 1; 10). The Copper Harbor Conglomerate fines upward and is conformable with the overlying shales, siltstones and sandstones of the Nonesuch Formation, which are the focus of this study. These lithologies of the Nonesuch Formation are interpreted as a lacustrine facies association (e.g. 22, 23) along a >250 km long belt in northern Michigan and Wisconsin (Fig. 1). Similar facies in drill core as far south as Iowa has led to an interpretation that Paleolake Nonesuch was >800 km long (24), although the extent of these lithofacies could be due to multiple lakes along the rift axis as in the modern East African Rift. Regardless, the lake in northern Wisconsin and Michigan was large and persistent with lacustrine sedimentation continuing until after the transition into the overlying Freda Formation. The Freda Formation is a >4 km thick succession that is dominantly comprised of channelized sandstone and overbank siltstone deposits representing a prolonged terrestrial fluvial environment (25). The Nonesuch Formation has been directly dated using Re-Os geochronology with a preferred date of 1078 ± 24 Ma (11). Paleomagnetic data from the Nonesuch Formation (26) suggest deposition in the tropics at a latitude of 3°± 3°.

Five drill cores from northern Wisconsin were used by (23) to develop a sequence stratigraphic framework for the Nonesuch Formation. Our work focuses on two of these cores: DO-8 and WC-9 (Figs. 1 and 2). In this region, the transgression that marks the flooding surface where alluvial facies of the Copper Harbor Conglomerate transition to the lacustrine facies of the Nonesuch Formation is followed by an interval of deep water lacustrine facies dominated by planar laminated siltstone and very-fine sandstone with intervals of thinly interbedded siltstone and carbonate (Fig. 2; 23). Following the maximum flooding of the lake, an aggradational-progradational sequence records a progressive shallowing sequence (Fig. 2). The Nonesuch Formation is transitional with the overlying Freda Formation and the formation boundary is typically set on the basis of color (23, 25). As a result, similar lithofacies deposited in a lacustrine environment are found on either side of the formation boundary with fluvial channel sandstone present higher in the Freda stratigraphy (Fig. 2).

That the Nonesuch Formation is conformable with underlying and overlying terrestrial sediments has been interpreted to imply that it was deposited in a terrestrial lake rather than a marine setting (e.g. 22, 27). However, the Nonesuch facies themselves could be consistent with either a lacustrine or protected marine depositional environment. Some workers have invoked incursion of marine waters into the basin based on interpretations of the affinity of putative sterane biomarkers (28; whose indigenous origin is called into question by data from (29) revealing modern contamination) and the presence of sulfides indicative of bacterial sulfate reduction (30). Given

that neither of these lines of evidence are diagnostic of a marine environment, the stratigraphic context of the formation and its position within an intracontinental rift favors a lacustrine depositional setting (22).

The Nonesuch Formation is exceptionally well-preserved, with maximum burial temperatures of 140-150°C estimated by modeled burial temperatures (31) and 125-155°C inferred from solid-state reordering modeling of clumped isotope values (32). In contrast to the Iron River syncline and Presque Isle Syncline (>100 km away; Fig. 1) where there is copper mineralization in the basal Nonesuch Formation, there is no mineralization in cores from the Ashland syncline (23, Fig. S1).

Iron speciation results. Geochemical analyses were performed to compare the DO-8 and WC-9 cores to previously published analyses from the Nonesuch Formation within the Presque Isle Syncline (Fig. 1). Iron speciation is a bulk sequential extraction technique that separates iron into distinct pools that are ratioed and compared to empirical calibrations on modern sediments in order to make interpretations of paleo-redox conditions (18, 33). Analyses proceeded using standard protocols (33, 34) with measurements of standards consistent with previous analyses (35). Our results for Fe_{HR}/Fe_T are generally below the common threshold of 0.38 used to separate likely oxic (<0.38) from anoxic (>0.38) depositional environments (18, 36) such that they fall in the range of equivocal values (0.2 to 0.38) or the oxic range (<0.2; Fig. 2). Samples falling in the equivocal zone could have been deposited under an oxygenated water column or could have been deposited in anoxic conditions but with processes masking Fe_{HR} enrichment, such as rapid sedimentation or burial diagenesis/metamorphism transforming highly reactive iron minerals into unreactive phases such as clay minerals (37, 38). The Fe_{py}/Fe_{HR} (pyrite iron to highly reactive iron) is elevated in lower portions of the formation, but still indicates that not all reactive iron was pyritized similar to the findings from the Presque Isle Syncline (11). Overall, these iron speciation ratios are ambiguous and elude straightforward interpretation of paleoredox.

Magnetic and petrographic results with interpretation. Experimentally determined estimates of magnetization and coercivity on samples spanning the stratigraphic sections (Figs. 2, 3), reveal three distinct magnetic facies within the Nonesuch Formation. Low-temperature magnetic experiments designed to elucidate low-temperature transitions confirm the ferromagnetic mineral identifications associated with these facies in both cores (Fig. S2, S3). Petrographic and microscale textural geochemical analyses on selected samples using transmitted light, reflected light, and electron microscopy paired with energy-dispersive X-ray spectroscopy (EDS) further confirm the magnetic mineralogy interpretations and give a more complete perspective of the mineralogy associated with each facies and the depositional and diagenetic processes they represent (Fig. 3, S7-S9).

Magnetic facies 1 is present in the deepest water lithologic facies and is characterized by a lack of hematite and a very weak magnetization carried by trace magnetite (Figs. 2, 3, S1, S2, S3). No magnetite could be seen using microscopy techniques, corroborating the low abundance and/or nanoscale size of these minerals. The iron within this facies is predominantly found in phyllosilicates, calcalumnosilicates, and abundant sulfides (Fig. 3, S7). Euhedral pyrite crystals range in size from <1 μm to 15 μm and can form aggregates up to 100 μm. Based on their shape and occasional textural association with iron-bearing clays, we interpret them to have formed in pore fluids from iron liberated from magnetite and clays during reductive dissolution and sulfidization (Fig. 3, S7). Facies 1 shows no evidence for oxidation of these reduced phases, highlighting the excellent preservation of these drill cores and lack of secondary oxidative fluid flow in this region. Titanium minerals—titanium oxide (rutile and/or anatase), leucoxene, and titanite—are found in samples of this facies, and texturally some appear to be authigenic (Fig. S7). Authigenic titanium-bearing minerals commonly form during dissolution of iron-bearing phases including titanomagnetite grains (42–44). Taken together these data indicate that the very weak magnetization relative to the other magnetic facies is the result of reductive dissolution of iron oxides, likely through a combination of dissimilatory iron reduction and sulfidization.

Magnetic facies 2 is characterized by a mixed assemblage of magnetite and hematite with relatively strong overall magnetization (Figs. 2, 3, S1, S2, S3). Microscale textural observations demonstrate the presence of detrital (titano)magnetite with igneous origins based on the exsolution between titanomagnetite and ilmenite (Fig. 3, S8). A sharply preserved Verwey transition revealed through low-temperature magnetometry indicates the presence of magnetite with no to minimal oxidation (Figs. S2, S3). The relatively high coercivity of the magnetite as revealed in coercivity spectra (Fig. 3), combined with the results of first-order reversal curve experiments (Figs. S5), are consistent with behavior dominated by small (<3 μm) vortex state grains (45). Detrital grains containing hematite are observed; the hematite is typically associated with, and replacing, phyllosilicates indicating oxidation during pre-transport weathering, riverine transport and/or deposition (Fig. 3, S8). The detrital nature of these grains is confirmed by their sometimes rounded shapes and the deformation of clay minerals between them and other detrital grains (Fig. S8). Pieces of organic matter (80 to 100 μm by 10 μm) with compaction warping are also preserved within this facies (Fig. S8). Some reductive dissolution of iron oxides may have occurred based on the presence of mixed mineral grains of titanite and iron oxides as well as minor amounts of pyrite (Fig. S8). However, in contrast with facies 1, the data show that such reductive dissolution was minimal and likely isolated to small regions of pore waters that became anoxic and sulfidic within the sediment. We interpret this mixed hematite and magnetite assemblage as a good representation of the detrital riverine input to the lake given that iron oxide grains were largely not reductively dissolved nor were magnetite grains fully oxidized to ferric oxide phases. The preservation of a detrital assemblage is therefore more consistent with persistent intermediate oxygen levels than fluctuations between anoxic and oxic conditions.

Magnetic facies 3 is present in the shallowest water sediments and is dominated by hematite with minimal contribution from lower coercivity phases such as magnetite (Figs. 2, 3, S2, S3). Microscale textural analyses reveal hematite that formed from oxidation of detrital igneous (titano)magnetite grains based on abundant titanohematite/titanomaghemite sometimes within rutile grains or with relict skeletal and trellis lamallae shapes (Fig. 3, S9). Additional hematite and titanohematite/titanomaghemite grains are seen as platelets within phyllosilicate grains or rimming quartz grains (Fig. S9).

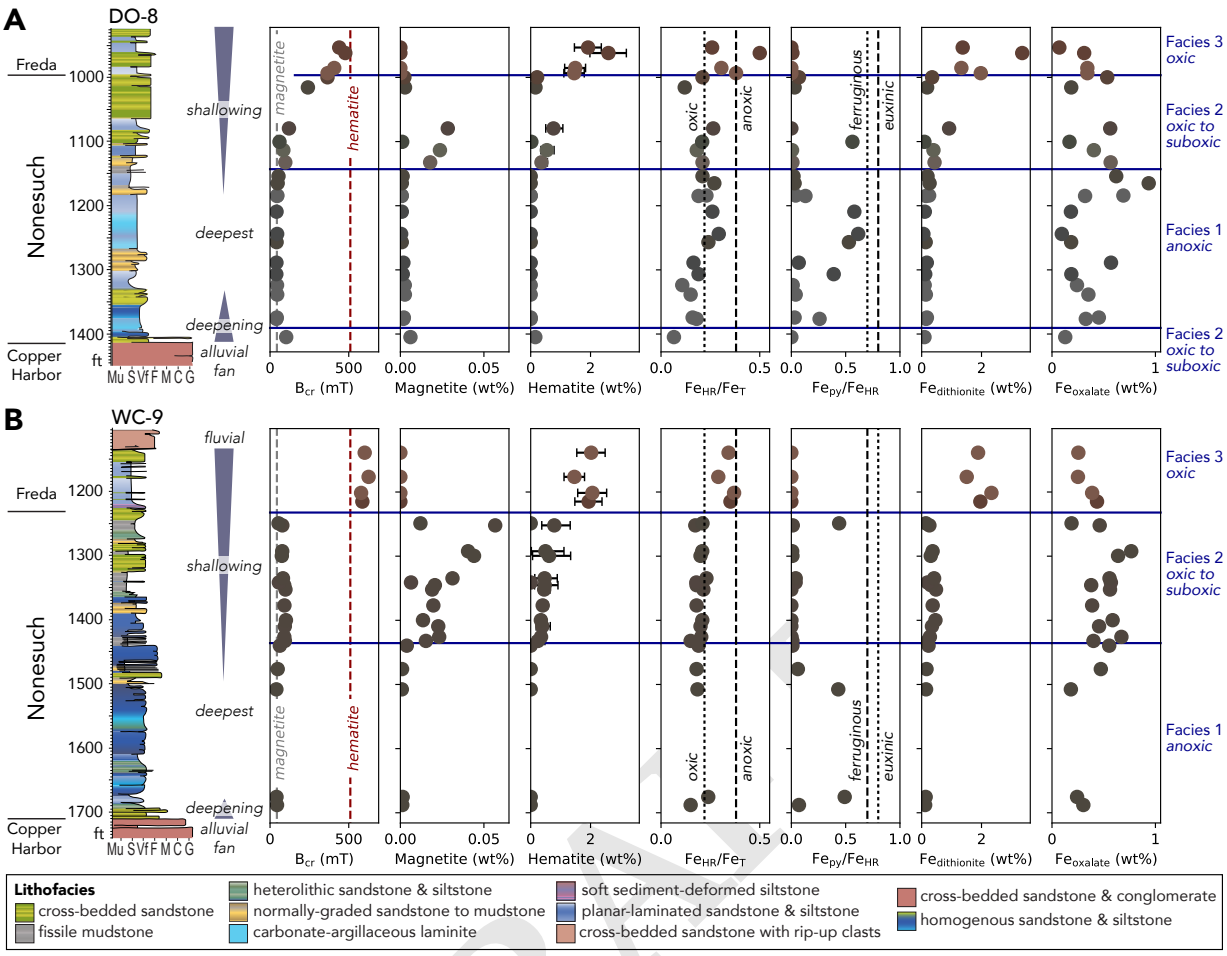

Fig. 2. Rock magnetic and iron speciation data from the DO-8 (A) and WC-9 (B) cores through the Nonesuch Formation. Lithostratigraphy is modified from (23) with additional measured section. Core depth is given in feet (1 ft = 0.3048 m) as those units are used for depth in the original cores. The grain size abbreviations are: Mu = mud, S = silt, Vf = very fine sandstone, F = fine sandstone, M = medium sandstone, C = coarse sandstone, G = granule to cobble conglomerate. The sequence stratigraphic interpretation of deepening and shallowing follows (22) and (23). Data points are colored reflecting the actual rock color. On the B_{cr} (coercivity of remanence) plot, the average coercivity values of hematite and magnetite are plotted for reference. Magnetite abundance is an upper bound calculated using the saturation magnetization value of well-characterized magnetite grains (39). Hematite abundance was calculated using either the saturation magnetization (when it is the only ferromagnetic phase present) or the remanent saturation magnetization and coercivity spectra. Range bars on these calculated values capture both one standard deviation uncertainty associated with coercivity spectra unmixing and the range of (remanent) saturation magnetization values measured in pure minerals (40, 41) (for more details see SI Appendix). The three distinct magnetic facies, composed of distinct magnetic mineral assemblages, are denoted by blue lines and labeled along with interpreted depositional redox conditions. In the Fe_{HR}/Fe_T and Fe_{py}/Fe_{HR} plots (HR—highly reactive; T—total; py—pyrite), vertical dashed lines denote boundaries for oxic versus anoxic and ferruginous versus euxinic water column conditions, respectively, that are utilized for iron speciation paleoredox proxy interpretations (18). While much of the Fe_{HR}/Fe_T data fall in the "equivocal" zone between anoxic or oxic conditions, the iron removed through each progressive extraction, particularly the $Fe_{dithionite}$ extraction, varies with the magnetic facies.

Titanite and leucoxene are frequently observed and authigenic titanium oxide grains were found, confirming that in-place oxidation of iron-titanium minerals occurred (Figs. 3, S9; 42). Petrography also shows that, in addition to the observed grains of hematite, there is abundant pigmentary hematite in facies 3 (Fig. S9). These data reveal that in this facies there has been significant oxidation of the detrital input to the lake both during transport and, due to the presence of pigmentary hematite and authigenic titanium oxides, within the sediment. The original detrital input appears to have been similar to facies 2 prior to additional oxidation.

Combined insights from magnetism and microscale textural analyses with iron speciation. While rock magnetism and petrography reveal that the iron mineralogy (and interpreted paleoredox) changes significantly through the cores, the Fe_{HR}/Fe_T ratios are rather uniform. The previous iron speciation study of Lake Nonesuch (11) interpreted their similar 'equivocal' Fe_{HR}/Fe_T ratios to be indicative of ferruginous environmental conditions obscured by post-depositional transformation of the Fe_{HR} pool into clays. A major driver of this interpretation was elevated Fe_T/Al ratios above normal oxic shale values (e.g. 0.53 ± 0.11; 46) and elevated iron abundance in poorly reactive silicates. Both of these enrichments were proposed to result from iron shuttling under anoxic conditions (11). The Fe_T/Al ratios determined for our samples (ranging from 0.57 to 0.99) are similar to these previous results (Fig. S1). However, maps of modern soil geochemistry reveal there is substantial variability in detrital Fe_T/Al ratios (19) and a lake setting within a volcanic province, such as Paleolake Nonesuch, is a setting where the Fe_T/Al ratio of the detrital flux is likely to be higher than average. The Fe_T/Al ratios in the oxic shallow sediments of facies 3, which should not

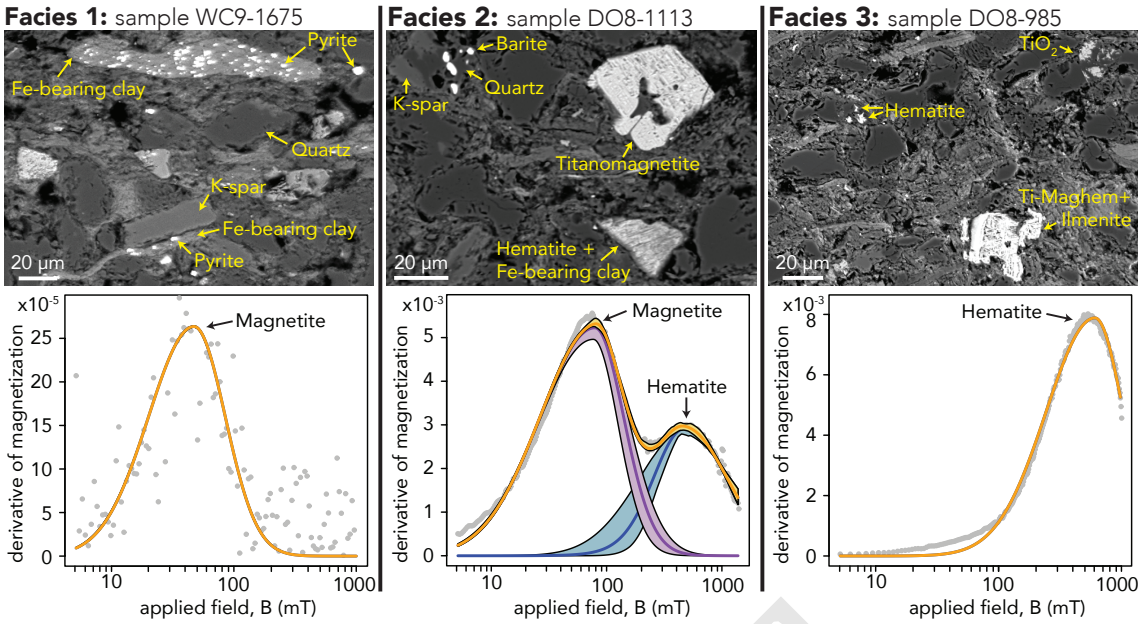

Fig. 3. Example back-scatter electron microscope images and bulk coercivity spectra from each magnetic facies. The coercivity spectra show the derivative of magnetization ($dM(Am^2)/dB$ (mT)) as a function of applied field and are fit with log-Gaussian components (40). The multiple components in facies 2 are unmixed and shown with uncertainty associated with the unmixing (40). Facies 1 is characterized by the presence of pyrite and a noisy coercivity spectrum due to weak magnetization that indicates the presence of magnetite in trace quantities (∼15 ppm in this sample). Facies 2 has detrital grains of titanomagnetite (igneous titanomagnetite with exsolution lamallae visible in image) and hematite with significant quantities of both magnetite and hematite resulting in a double-peaked coercivity spectrum. Facies 3 has a coercivity spectrum dominated by hematite with disseminated hematite, aggregates of hematite crystals, and oxidized detrital titanomagnetite grains visible via electron microscopy.

have experienced authigenic enrichments, are similar to those within the other facies (Fig. S1). These data support an interpretation that the Fe_T/Al ratio is representative of the detrital flux into Paleolake Nonesuch rather than the result of enrichment of iron from an anoxic water column.

Although the Fe_{HR}/Fe_T ratios themselves may be ambiguous and lack a clear correlation to the three magnetic facies, if the iron extraction pools are looked at in detail considerable differences are noted, which also separate the section into three facies (Figs. 2, S1). Facies 3 stands out as having high $Fe_{dithionite}$, low $Fe_{acetate}$, and low Fe_{CRS}; the dithionite extraction targets ferric iron (hydr)oxides which agrees well with our magnetic quantification of abundant hematite in this facies. While hematite is the most oxidized endmember within the ulvospinel-magnetite-ilmenite-hematite series and forms within oxidizing environments, in iron speciation analysis it is grouped with the highly reactive phases. Therefore, its presence increases Fe_{HR}/Fe_T, which is higher in oxic facies 3 than the other facies and contains the only sample with $Fe_{HR}/Fe_T > 0.38$. This high Fe_{HR}/Fe_T value could erroneously lead to the interpretation of an anoxic environment if the mineralogy leading to this high value were not considered. Facies 1 has relatively low $Fe_{dithionite}$ and high Fe_{CRS}, which agrees with magnetic analyses suggesting no hematite and petrographic observations of pyrite (extracted as chromium reducible sulfur, CRS) in these samples. While the $Fe_{oxalate}$ pool is typically attributed to magnetite such that it is sometimes called Fe_{mag} (33), facies 1, 2 and 3 have similar $Fe_{oxalate}$ values even though the magnetic and textural analyses show facies 2 to have much more magnetite. The quantity of iron in the oxalate extraction is one to three orders of magnitude higher than the abundance of magnetite calculated utilizing the magnetic data (Fig. S10), and quantities of magnetite approaching 1 wt% in a shale would be highly unusual. These results indicate that the oxalate extraction is solubilizing iron from other minerals in addition to magnetite. More research is needed to fully understand the mineralogy removed by each sequential extraction step in natural samples. In the meantime, workers should continue to utilize careful terminology to make it clear that this is an operational definition and that much of the iron in the oxalate extraction is not from magnetite. Considering the sequential iron speciation extraction data from (11) in a similar framework would place most of those analyses in facies 1 with zones of facies 3 and 2 near the basal flooding surface with the Copper Harbor Conglomerate. As less than half of the thickness of the Nonesuch Formation was captured in the Presque Isle drill-core (47) from which these data were obtained, such a classification matches our interpretations.

A preserved oxycline. These three facies and their juxtaposition can be explained as the result of an oxycline in the lake. The detrital input to the lake included both magnetite and hematite (preserved in facies 2) due to weathering and oxidation of the source igneous material during transport. Sediments in the deepest part of the lake were anoxic, possibly with anoxia extending into the water column; as a result, delivered iron oxides underwent reductive dissolution through microbial metabolic processes as recorded by facies 1. Much of this iron and iron within sheet silicates reacted with sulfide to form pyrite, but sulfide availability was restricted to pore waters and not sufficient to sulfidize all the available reactive iron. Intermediate oxygen levels in waters throughout much of the lake allowed for the preservation of detrital magnetite and hematite in facies 2. In the shallow waters of the lake recorded in facies 3, oxic conditions prevailed and most of the detrital magnetite, as well as iron in other phases, was oxidized to

hematite.

We interpret this vertical sequence of facies to reflect a stacking of laterally distributed environments such that the transition from the deepest-water low-iron-oxide facies into the intermediate-water magnetite-rich facies and the shallower-water hematite-rich facies is the result of an oxycline within the ancient lake. The depth dependence of the oxycline is similar to that found in modern eutrophic lakes wherein the aerobic respiration of descending organic matter leads to a decrease in dissolved oxygen with depth. Overall, these data indicate that the lake was more deeply oxygenated than has previously been interpreted on the basis of iron speciation data alone. For much of its temporal duration, and throughout much of its water column, there was oxygen in the waters of Paleolake Nonesuch. While trophic modes are poorly known for the diverse biota found within the Nonesuch (4) and their paleobathymetric distribution is poorly constrained, these eukaryotes lived in a stable and hospitable lake environment with available oxygen. It remains a puzzle why these eukaryotic denizens in the fossil record did not leave an appreciable sterane record (29) and why, despite seemingly favorable environmental conditions, eukaryotic productivity was so low that sterane/hopane ratios have been found to be zero in indigenous organic matter (48). Regardless, the environmental signal from this diverse lacustrine fossil locality is becoming clear. Overall, these results highlight that coupling magnetic and microscale textural data with geochemical data can resolve ambiguous redox interpretations in deep time.

ACKNOWLEDGMENTS. This research was supported by the Esper S. Larsen Jr. Research Fund and the Miller Institute for Basic Science. Many of the rock magnetic experiments were conducted during a visiting fellowship at the Institute for Rock Magnetism which is supported by the National Science Foundation and the University of Minnesota. Esther Stewart and Valerie Stanley provided support and guidance at the Wisconsin Geological and Natural History Survey core repository. Luke Fairchild assisted with geological data compilation, Sabrina Tecklenburg assisted with iron speciation analyses, and Malcolm Hodgskiss, Ioan Lascu, and Bruce Moskowitz provided useful insights regarding interpretations.

1. Knoll AH (2014) Paleobiological perspectives on early eukaryotic evolution. *Cold Spring Harbor Perspectives in Biology* 6(1):a016121–a016121.
2. Cohen PA, Macdonald FA, Pruss S, Matys E, Bosak T (2015) Fossils of putative marine algae from the Cryogenian glacial interlude of Mongolia. *PALAIOS* 30(3):238–247.
3. Lyons TW, Reinhard CT, Love GD, Xiao S (2012) Geobiology of the Proterozoic Eon. *Fundamentals of Geobiology* pp. 371–402.
4. Wellman CH, Strother PK (2015) The terrestrial biota prior to the origin of land plants (embryophytes): a review of the evidence. *Palaeontology* 58(4):601–627.
5. Hardisty DS, et al. (2017) Perspectives on Proterozoic surface ocean redox from iodine contents in ancient and recent carbonate. *Earth and Planetary Science Letters* 463:159–170.
6. Porter SM, Agić H, Riedman LA (2018) Anoxic ecosystems and early eukaryotes. *Emerging Topics in Life Sciences* p. ETLS20170162.
7. Butterfield NJ (2017) Oxygen, animals and aquatic bioturbation: An updated account. *Geobiology* 16(1):3–16.
8. Strother PK, Battison L, Brasier MD, Wellman CH (2011) Earth's earliest non-marine eukaryotes. *Nature* 473(7348):505–509.
9. Nicholson SW, Dicken CL, Foose MP, Mueller JAL (2004) Preliminary integrated geologic map databases for the United States: Minnesota, Wisconsin, Michigan, Illinois, and Indiana, (U.S. Geological Survey), U.S. Geological Survey Open-File Report.
10. Fairchild LM, Swanson-Hysell NL, Ramezani J, Sprain CJ, Bowring SA (2017) The end of Midcontinent Rift magmatism and the paleogeography of Laurentia. *Lithosphere* 9(1):117–133.
11. Cumming VM, Poulton SW, Rooney AD, Selby D (2013) Anoxia in the terrestrial environment during the late Mesoproterozoic. *Geology* 41(5):583–586.
12. Swanson-Hysell NL, Ramezani J, Fairchild LM, Rose I (2018) Failed rifting and fast drifting: Midcontinent Rift development, Laurentia's rapid motion and the driver of Grenvillian orogenesis. *Geological Society of America Bulletin* p. 10.1130/B31944.1.
13. Strother PK, Wellman CH (2016) Palaeoecology of a billion-year-old non-marine cyanobacterium from the Torridon Group and Nonesuch Formation. *Palaeontology* 59(1):89–108.
14. Javaux EJ (2011) Early eukaryotes in Precambrian oceans in *Origins and Evolution of Life: An Astrobiological Perspective.* (Cambridge University Press).
15. Parnell J, Boyce AJ, Mark D, Bowden S, Spinks S (2010) Early oxygenation of the terrestrial environment during the Mesoproterozoic. *Nature* 468(7321):290–293.
16. Sim MS, Bosak T, Ono S (2011) Large sulfur isotope fractionation does not require disproportionation. *Science* 333(6038):74–77.
17. Leavitt WD, Halevy I, Bradley AS, Johnston DT (2013) Influence of sulfate reduction rates on the Phanerozoic sulfur isotope record. *Proceedings of the National Academy of Sciences* 110(28):11244–11249.
18. Poulton SW, Canfield DE (2011) Ferruginous conditions: A dominant feature of the ocean through earth's history. *Elements* 7(2):107–112.
19. Cole DB, Zhang S, Planavsky NJ (2017) A new estimate of detrital redox-sensitive metal concentrations and variability in fluxes to marine sediments. *Geochimica et Cosmochimica Acta* 215:337–353.
20. Cannon WF, Hinze WJ (1992) Speculations on the origin of the North American Midcontinent rift. *Tectonophysics* 213(1-2):49–55.
21. Elmore RD (1984) The Copper Harbor Conglomerate: A late Precambrian fining-upward alluvial fan sequence in northern Michigan. *Geological Society of America Bulletin* 95(5):610–617.
22. Elmore R, Milavec GJ, Imbus SW, Engel MH (1989) The Precambrian Nonesuch Formation of the North American Mid-Continent Rift, sedimentology and organic geochemical aspects of lacustrine deposition. *Precambrian Research* 43(3):191–213.
23. Stewart EK, Mauk JL (2017) Sedimentology, sequence-stratigraphy, and geochemical variations in the Mesoproterozoic Nonesuch Formation, northern Wisconsin, USA. *Precambrian Research* 294:111–132.
24. Anderson RR (1997) *Middle Proterozoic to Cambrian rifting, central North America*, eds. Ojakangas RW, Dickas AB, Green JC. (Geological Society of America) Vol. 312, pp. 211–230.
25. Ojakangas RW, Morey GB, Green JC (2001) The Mesoproterozoic Midcontinent Rift System, Lake Superior Region, USA. *Sedimentary Geology* 141-142:421–442.
26. Henry S, Mauk F, Van der Voo R (1977) Paleomagnetism of the upper Keweenawan sediments: Nonesuch Shale and Freda Sandstone. *Canadian Journal of Earth Science* 14:1128–1138.
27. Pettijohn FJ (1957) *Sedimentary rocks.* (Harper and Row).
28. Pratt LM, Summons RE, Hieshima GB (1991) Sterane and triterpane biomarkers in the Precambrian Nonesuch Formation, North American Midcontinent Rift. *Geochimica et Cosmochimica Acta* 55(3):911–916.
29. Brocks JJ, Grosjean E, Logan GA (2008) Assessing biomarker syngeneity using branched alkanes with quaternary carbon (BAQCs) and other plastic contaminants. *Geochimica et Cosmochimica Acta* 72(3):871–888.
30. Hieshima G, Pratt L (1991) Sulfur/carbon ratios and extractable organic matter of the middle Proterozoic Nonesuch Formation, North American Midcontinent Rift. *Precambrian Research* 54(1):65–79.
31. Mauk JL, Hieshima GB (1992) Organic matter and copper mineralization at White Pine, Michigan, U.S.A. *Chemical Geology* 99(1):189–211.
32. Gallagher TM, et al. (2017) Constraining the thermal history of the North American Midcontinent Rift System using carbonate clumped isotopes and organic thermal maturity indices. *Precambrian Research* 294:53–66.
33. Poulton SW, Canfield DE (2005) Development of a sequential extraction procedure for iron: implications for iron partitioning in continentally derived particulates. *Chemical Geology* 214(3–4):209–221.
34. Canfield DE, Raiswell R, Westrich JT, Reaves CM, Berner RA (1986) The use of chromium reduction in the analysis of reduced inorganic sulfur in sediments and shales. *Chemical Geology* 54(1-2):149–155.
35. Sperling EA, et al. (2015) Statistical analysis of iron geochemical data suggests limited late Proterozoic oxygenation. *Nature* 523(7561):451–454.
36. Raiswell R, Canfield DE (1998) Sources of iron for pyrite formation in marine sediments. *American Journal of Science* 298(3):219–245.
37. Slotznick SP, Eiler JM, Fischer WW (2018) The effects of metamorphism on iron mineralogy and the iron speciation redox proxy. *Geochimica et Cosmochimica Acta* 224:96–115.
38. Raiswell R, et al. (2018) The iron paleoredox proxies: A guide to the pitfalls, problems and proper practice. *American Journal of Science* 318(5):491–526.
39. Dunlop DJ (1986) Hysteresis properties of magnetite and their dependence on particle size: A test of pseudo-single-domain remanence models. *Journal of Geophysical Research* 91(B9):9569–9584.
40. Maxbauer DP, Feinberg JM, Fox DL (2016) MAX UnMix: A web application for unmixing magnetic coercivity distributions. *Computers and Geosciences* 95:140–145.
41. Özdemir Ö, Dunlop DJ (2014) Hysteresis and coercivity of hematite. *Journal of Geophysical Research: Solid Earth* 119(4):2582–2594.
42. Morad S, Aldahan AA (1982) Authigenesis of titanium minerals in two Proterozoic sedimentary rocks from southern and central Sweden. *Journal of Sedimentary Research* 52(4):1295–1305.
43. Morad S (1988) Diagenesis of titaniferous minerals in Jurassic sandstones from the Norwegian Sea. *Sedimentary Geology* 57(1-2):17–40.
44. van Panhuys-Sigler M, Trewin NH (1990) Authigenic sphene cement in Permian sandstones from Arran. *Scottish Journal of Geology* 26(2):139–144.
45. Lascu I, Einsle JF, Ball MR, Harrison RJ (2018) The vortex state in geologic materials: A micromagnetic perspective. *Journal of Geophysical Research: Solid Earth* p. 10.1029/2018jb015909.
46. Raiswell R, et al. (2008) Turbidite depositional influences on the diagenesis of Beecher's Trilobite Bed and the Hünsruck Slate; sites of soft tissue pyritization. *American Journal of Science* 308(2):105–129.
47. Nielsen R (1958) PI-1 and PI-2 drill logs, (Bear Creek Mining Company), Technical report.
48. Gueneli N, et al. (2018) 1.1-billion-year-old porphyrins establish a marine ecosystem dominated by bacterial primary producers. *Proceedings of the National Academy of Sciences* 115(30):E6978–E6986.